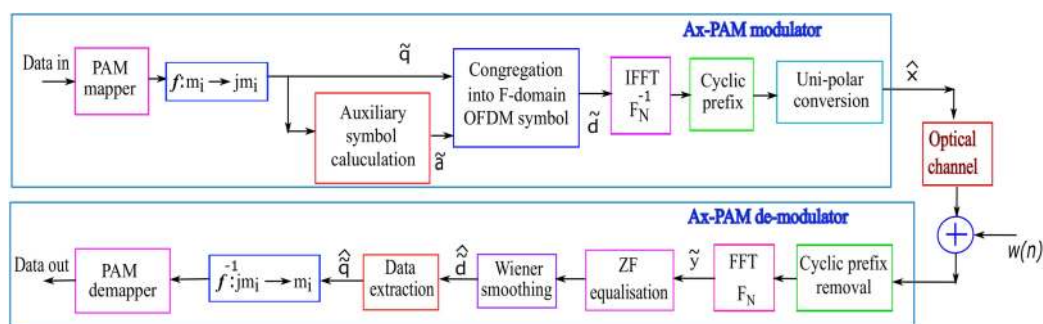


# A Tunable Energy Signal for Intensity Modulation and Direct Detection Systems: Theory, Simulations, and Experiments



Volume 12, Number 1, February 2020

Kishore Vejandla, *Student Member, IEEE*  
Sivaprasad Valluri, *Student Member, IEEE*  
V. Mani Vakamulla, *Senior Member, IEEE*  
Abhinav Kumar, *Member, IEEE*



DOI: 10.1109/JPHOT.2019.2958836

# A Tunable Energy Signal for Intensity Modulation and Direct Detection Systems: Theory, Simulations, and Experiments

Kishore Vejandla <sup>1</sup>, *Student Member, IEEE*,  
Sivaprasad Valluri,<sup>1</sup> *Student Member, IEEE*,  
V. Mani Vakamulla <sup>1</sup>, *Senior Member, IEEE*,  
and Abhinav Kumar,<sup>2</sup> *Member, IEEE*

<sup>1</sup>Department of Electronics and Communication Engineering, National Institute of Technology, Warangal, Warangal 506004, India

<sup>2</sup>Department of Electrical Engineering, Indian Institute of Technology Hyderabad, Hyderabad 502285, India

DOI:10.1109/JPHOT.2019.2958836

This work is licensed under a Creative Commons Attribution 4.0 License. For more information, see <https://creativecommons.org/licenses/by/4.0/>

Manuscript received November 4, 2019; revised November 28, 2019; accepted December 4, 2019. Date of publication December 10, 2019; date of current version January 7, 2020. This work was supported in part by the Science and Engineering Research Board (SERB) under Grant EMR/2016/7687, New Delhi, in part by the Ministry of Human Resource Development (MHRD)-Government of India for awarding the Grant under SPARC 2019/249, and in part by the Department of Science and Technology (DST), Government of India under Grant TMD/CERI/BEE/2016/059(G). Corresponding author: Kishore Vejandla (e-mail: kishorevejandla@student.nitw.ac.in).

**Abstract:** In this paper, we propose a novel method to generate real signal for Visible Light Communication (VLC) systems without using traditional hermitian symmetry on the data symbols obtained using M-ary Pulse Amplitude Modulation (PAM) which is named as Auxiliary PAM (Ax-PAM). We mathematically analyse this method to generate a real signal with tunable energy using auxiliary symbols at the transmitter and the corresponding receiver. Simulation results for Bit Error Rate (BER) show better performance over conventional PAM Discrete Multi-Tone (PAM-DMT) and Asymmetrically Clipped Optical Orthogonal Frequency Division Multiplexing (ACO-OFDM) even under clipping distortion and also demonstrate the tunable energy for the proposed scheme. Furthermore, the proposed scheme is implemented on a VLC test bed designed using Universal Software defined Radio Peripheral (USRP). The experimental results for estimated Signal to Noise Ratio (SNR) and achieved BER for Ax-PAM outperforms PAM-DMT and ACO-OFDM.

**Index Terms:** Asymmetrically clipped optical orthogonal frequency division multiplexing (ACO-OFDM), bit error rate (BER), pulse amplitude modulated discrete multi-tone (PAM-DMT), visible light communication (VLC).

## 1. Introduction

The surge in the demand for the high data rates has made the researchers to consider the Visible Light Communications (VLC) as an alternative to Radio Frequency (RF) communications. Along with huge bandwidth, the high speed switching property of Light Emitting Diodes (LED) has made VLC as an appropriate option to simultaneously offer communication and illumination. For transmitting information, a VLC system relies on Intensity Modulation (IM) and Direct Detection (DD) principle, due to which the transmitted signal is constrained to be unipolar. Hence, Orthogonal Frequency Division Multiplexing (OFDM) used for RF communication is not suitable directly for

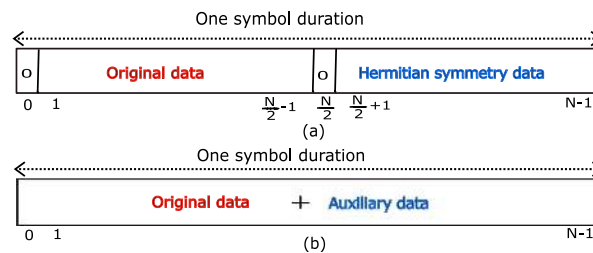


Fig. 1. Arrangement of symbols in frequency domain in (a) traditional hermitian symmetry based systems and (b) Ax-PAM.

VLC systems. Several variants of multi-carrier modulation waveforms based on OFDM have been proposed in the literature to serve for the necessities of VLC systems in terms of signal type, signal power, and spectrum efficiency. Among all the optical OFDM types explored for IM/DD systems, DC-biased Optical OFDM (DCO-OFDM), Asymmetrically Clipped Optical OFDM (ACO-OFDM), and Pulse Amplitude Modulated Discrete Multi-Tone (PAM-DMT) are some of the important contributions [1], [2]. Among these, DCO-OFDM is inefficient in terms of power, whereas, ACO-OFDM lags in spectral efficiency. Additionally, the Peak-to-Average Power Ratio (PAPR) of these OFDM based modulations is high which increases non-linear clipping distortion at the LED transmitter. Thus, PAM-DMT has been explored for IM/DD systems, but it also employs hermitian symmetry on the data symbols to attain the real signal in time domain. Even though some hybrid OFDM based waveforms are implemented for wireless VLC over fiber, the non linearity distortion remain uncontrolled [3], [4]. In [5], [6], Unique Word (UW)-OFDM is proposed for RF systems to improve performance by improving the correlation among the data symbols. [7], [8] applied the UW-OFDM to IM/DD systems, but to obtain the real signal they rely on hermitian symmetry. Further, along with symmetrical symbols, a separate UW is also required to be sent in [7], [8]. The time domain signal obtained in the above methods cannot be properly tuned in terms of energy because of the inevitable symmetry on the data symbols in frequency domain. Motivated by this, we propose a new method for the generation of time domain real signal, energy of which can be controlled for PAM modulation and is named as Auxiliary PAM (Ax-PAM) modulation.

In Ax-PAM modulation, the original data symbols utilise auxiliary symbols instead of Hermitian symmetric data symbols to produce real signal. The generation of auxiliary symbols is explained in subsequent section. The data symbols and auxiliary symbols are placed on available sub-carriers according to a predefined pattern. The difference between arrangement of data symbols in traditional hermitian symmetry based systems and proposed scheme is shown in Fig. 1. In the traditional schemes, the position matrix is fixed to obtain the symmetry in the data symbols, whereas in the proposed scheme, the position matrix is random which places the auxiliary symbols on any available sub-carrier. Apart from this, we utilized Universal Software Radio Peripheral (USRP) based VLC test bed for the validation of the proposed scheme. In our previous works, we also have implemented Generalised Frequency Division Multiplexing (GFDM) based RF prototypes using USRP devices and Lab-view software platform [9]–[11]. Therefore, the proposed method also has been implemented and validated through the VLC test bed designed using USRPs hardware and Lab-view software in the present work.

The contributions of the proposed work are as follows.

- A tunable energy real signal is proposed for IM/DD systems using PAM modulation without hermitian symmetry.
- The proposed scheme is implemented and validated on a VLC test bed designed using USRPs and National instruments Lab-view software.
- We present and compare the simulation results for Bit Error Rate (BER) for the proposed scheme with traditional methods under clipping distortion.
- Experimental results for estimated Signal to Noise Ratio (SNR) at receiver at various energies and achieved BER for the proposed scheme are compared with state-of-the-art methods.

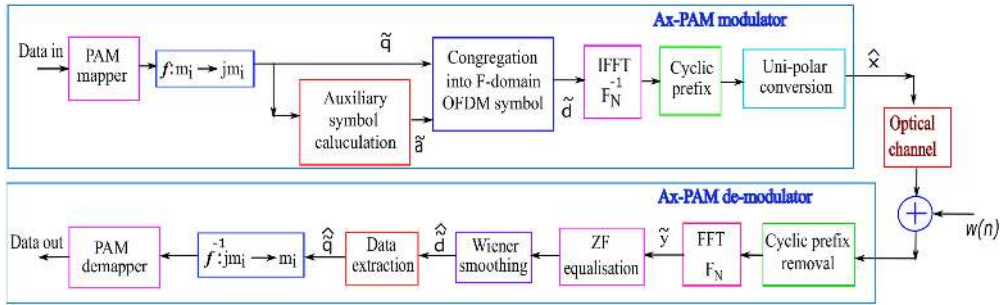


Fig. 2. Block diagram of Ax-PAM implementation for IM/DD systems.

- The real time channel frequency response under which experiments are carried out, is computed and depicted.

The rest of the paper is organised as follows. Section 2 presents the system model considered in this work including the transmitter and receiver structures. The simulation and experimental results are discussed in Section 3 and Section 4, respectively. Section 5 gives some concluding remarks.

## 2. System Model

In this section, we describe the system model whose block diagram is shown Fig. 2. Transmitter and receiver operations are explained analytically where as the channel model is considered from our previous work [12].

### 2.1 Transmitter

In a conventional PAM-DMT system, the real signal is obtained by employing Inverse Fast Fourier Transform (IFFT) on hermitian symmetry imposed data symbols  $\tilde{\mathbf{d}} \in \mathbb{C}^{N \times 1}$ . This can be represented in matrix form as  $\mathbf{x} = \mathbf{F}_N^{-1} \tilde{\mathbf{d}}$ , where,  $\mathbf{x} \in \mathbb{R}^{N \times 1}$  are the time domain samples and  $\mathbf{F}_N^{-1}$  is an  $N$ -point IFFT matrix. In contrast to this, we propose a new scheme to modify the data vector that yield real signal for IM/DD systems. In the proposed scheme, instead of the data symbols with hermitian symmetry, symbols  $\tilde{\mathbf{d}} \in \mathbb{C}^{N \times 1}$  that are applied to IFFT are formed by suitably placing auxiliary symbols  $\tilde{\mathbf{a}} \in \mathbb{C}^{N_m \times 1}$  and data symbols  $\tilde{\mathbf{q}} \in \mathbb{C}^{N_m \times 1}$  onto  $N$  sub-carriers according to a predetermined random position matrix  $\mathbf{P} \in \mathbb{C}^{(2N_m) \times (2N_m)}$ . The auxiliary symbols  $\tilde{\mathbf{a}}$  used to generate real signal are generated algebraically using the data symbols  $\tilde{\mathbf{q}}$  which is illustrated in Fig. 2. Unlike in the traditional approach where the symmetry symbols are appended at the last sub-carriers without having any control over the symbols, the proposed method gives control over the auxiliary symbols energy and can be allocated to any sub-carrier. The frequency domain interpretation of DMT symbol in vector form is given by,

$$\tilde{\mathbf{d}} = \mathbf{P} \begin{bmatrix} \tilde{\mathbf{q}} \\ \tilde{\mathbf{a}} \end{bmatrix}. \quad (1)$$

This vector  $\tilde{\mathbf{d}}$  which is constrained to produce real DMT symbol in time domain will form the required problem as,

$$\mathbf{F}_N^{-1} \mathbf{P} \begin{bmatrix} \tilde{\mathbf{q}} \\ \tilde{\mathbf{a}} \end{bmatrix} = \mathbf{x}, \text{ where, } \mathbf{x} \in \mathbb{R}^{N \times 1}. \quad (2)$$

We can rewrite (2) as,

$$\begin{bmatrix} \mathbf{E11} & \mathbf{E12} \\ \mathbf{E21} & \mathbf{E22} \end{bmatrix} \begin{bmatrix} \tilde{\mathbf{q}} \\ \tilde{\mathbf{a}} \end{bmatrix} = \mathbf{x}, \text{ where, } \mathbf{x} \in \mathbb{R}^{N \times 1} \quad (3)$$

and  $\mathbf{E} = \mathbf{F}_N^{-1} \mathbf{P} = \begin{bmatrix} \mathbf{E}_{11} & \mathbf{E}_{12} \\ \mathbf{E}_{21} & \mathbf{E}_{22} \end{bmatrix}$  with  $\mathbf{E}_{ij}$  being an appropriately adjusted sub matrix of  $\mathbf{E}$ . To attain a real signal  $\mathbf{x}$  from (3), the imaginary component that results on left side must be nullified. For a more clear interpretation, (3) is expressed as,

$$\left\{ \Re \begin{bmatrix} \mathbf{E}_{11} & \mathbf{E}_{12} \\ \mathbf{E}_{21} & \mathbf{E}_{22} \end{bmatrix} + \Im \begin{bmatrix} \mathbf{E}_{11} & \mathbf{E}_{12} \\ \mathbf{E}_{21} & \mathbf{E}_{22} \end{bmatrix} \right\} \begin{bmatrix} \tilde{\mathbf{q}} \\ \tilde{\mathbf{a}} \end{bmatrix} = \mathbf{x} \text{ where } \mathbf{x} \in \mathbb{R}^{N \times 1} \quad (4)$$

where  $\Re[\cdot]$  and  $\Im[\cdot]$  are real and imaginary parts of components inside. Now since the data vector  $[\tilde{\mathbf{q}}]$  is assumed to be formed by the transformation  $\{f : m_i \rightarrow jm_i\}$  where  $m_i$  is the  $i$ th symbol from M-PAM constellation, the vector  $[\tilde{\mathbf{q}}]$  is purely imaginary. Further, it is considered that the data symbols  $\tilde{\mathbf{q}}$  are uncorrelated and having zero mean with variance  $\sigma_q^2$ . Therefore, to yield the required real signal for IM/DD systems, imaginary term in (4) should be zero as follows.

$$\Re \begin{bmatrix} \mathbf{E}_{11} & \mathbf{E}_{12} \\ \mathbf{E}_{21} & \mathbf{E}_{22} \end{bmatrix} \begin{bmatrix} \tilde{\mathbf{q}} \\ \tilde{\mathbf{a}} \end{bmatrix} = \begin{bmatrix} \mathbf{0} \\ \mathbf{0} \end{bmatrix} \quad (5)$$

The expression in (5) produces two equations that yield two different possible solutions for calculation of auxiliary symbols.

$$\begin{aligned} \Re[\mathbf{E}_{11}] \tilde{\mathbf{q}} + \Re[\mathbf{E}_{12}] \tilde{\mathbf{a}} &= \mathbf{0} \\ \Re[\mathbf{E}_{21}] \tilde{\mathbf{q}} + \Re[\mathbf{E}_{22}] \tilde{\mathbf{a}} &= \mathbf{0} \end{aligned} \quad (6)$$

From the above equations, we can determine the auxiliary symbols utilising the following linear mapping

$$\tilde{\mathbf{a}} = \mathbf{T} \tilde{\mathbf{q}}, \quad (7)$$

where, the matrix  $\mathbf{T} = -\Re[\mathbf{E}_{12}]^{-1} \Re[\mathbf{E}_{11}]$  or  $-\Re[\mathbf{E}_{22}]^{-1} \Re[\mathbf{E}_{21}]$ ,  $\mathbf{T} \in \mathbb{C}^{N_m \times N_m}$  which is determined from (6) and (7) describes the generation of auxiliary symbols  $\tilde{\mathbf{a}}$  using data symbols  $\tilde{\mathbf{q}}$ . These auxiliary symbols when combined with data symbols  $\tilde{\mathbf{q}}$  according to position matrix  $\mathbf{P}$  as per (1), will result in

$$\tilde{\mathbf{d}} = \mathbf{P} \begin{bmatrix} \tilde{\mathbf{q}} \\ \mathbf{T} \tilde{\mathbf{q}} \end{bmatrix} = \mathbf{P} \begin{bmatrix} \mathbf{I} \\ \mathbf{T} \end{bmatrix} \tilde{\mathbf{q}} = \mathbf{Q} \tilde{\mathbf{q}}, \quad (8)$$

in which the matrix  $\mathbf{Q} \in \mathbb{C}^{(2N_m) \times N_m}$  is the generator matrix. Additionally, it is considered that in the absence of null carriers  $N = 2N_m$ , it turns out that the time domain OFDM symbol to be  $\mathbf{x} = \mathbf{F}_N^{-1} \tilde{\mathbf{d}}$ . For a Ax-PAM symbol with 4-PAM and  $N_m = 16$ , Fig. 3(a) shows the data symbols along with zeros indicating the position of auxiliary symbols and Fig. 3(b) shows both data symbols and auxiliary symbols in frequency domain. In Fig. 3(c) corresponding time domain signal is plotted. The prime contribution of this work is not only to generate real signal for IM/DD systems, but also to have a proper control over the mean energy  $E = \mathbb{E}[\mathbf{x}^H \mathbf{x}]$  of the real signal which can be obtained the following expression.

$$E = \frac{1}{N} \left( N_m \sigma_q^2 + \sigma_q^2 \text{tr}(\mathbf{T} \mathbf{T}^H) \right) \quad (9)$$

From (9), is observed that the mean energy  $E$  can be minimized by minimizing the cost function

$$C = \text{tr}(\mathbf{T} \mathbf{T}^H), \quad (10)$$

which in turn needs the proper selection of  $\mathbf{P}$  matrix. This is accomplished by utilising the proposed Algorithm 1 presented next. The Alg. 1. start by selecting  $i_a$  and  $i_q$  randomly anywhere from  $0, 1, \dots, N - 1$  which signifies the position of auxiliary and data symbols, respectively. A heuristic approach [13], is followed to repeat the procedure iteratively until a  $\mathbf{P}$  matrix is obtained with minimum cost function  $C$ .

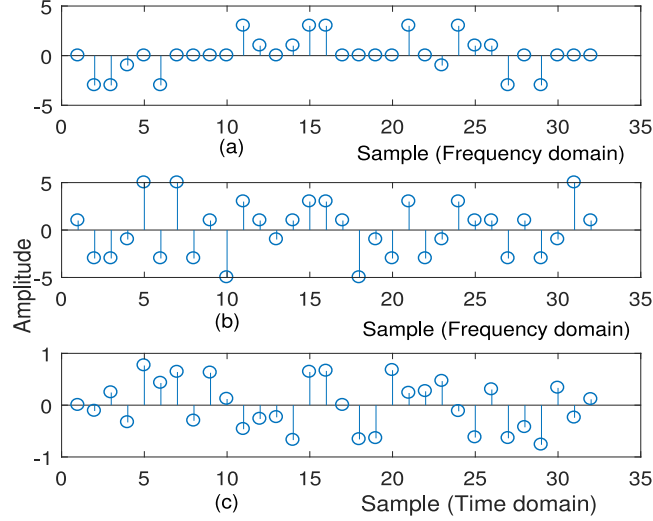


Fig. 3. Plot shows (a) only data symbols ( $\mathcal{J}[\tilde{q}]$ ) with zeros indicating position of auxiliary symbols. (b) A Ax-PAM symbol in frequency domain with both data and auxiliary symbols. (c) Corresponding Ax-PAM time domain symbol.

---

**Algorithm 1: Algorithm to Select Optimal Position Matrix ( $\mathbf{P}$ ).**

---

- 1: Choose valid position index vectors  $i_q$  and  $i_a$  randomly
  - 2: Assign  $C_{old} \leftarrow \text{inf}$ ,  $i \leftarrow \text{iterations}$ ,  $\mathbf{P}_{ini} \leftarrow \mathbf{P}$  (determined from step:1)
  - 3: **for**  $i \geq 0$  **do**
  - 4:      $i \leftarrow i - 1$
  - 5:     Calculate  $\mathbf{E}$  using  $\mathbf{P}$  and segregate submatrices. Eq. (3)
  - 6:     **if** ( $\mathbf{E}_{12}$  or  $\mathbf{E}_{22}$  non-singular) **then**
  - 7:         Calculate  $\mathbf{T}$ ,  $\mathbf{Q}$  and cost function  $C$ . Eq. (7), (8) and (10)
  - 8:         **if**  $C < C_{old}$  **then**
  - 9:             Assign  $C_{old} \leftarrow C$ ,  $\mathbf{P}_{opt} \leftarrow \mathbf{P}$
  - 10:         **else**
  - 11:             Sort  $i_q$  and  $i_a$ , determine new  $\mathbf{P}$  and go to step:3
  - 12:         **end if**
  - 13:     **else**
  - 14:         go to Step:11
  - 15:     **end if**
  - 16: **end for**
  - 17: Assign  $C_{opt} \leftarrow C_{old}$  and return  $\mathbf{P}_{opt}$
- 

## 2.2 Receiver

The DC added signal transmitted over the VLC channel modelled as in [12], [14] considering Line of Sight (LOS) path will be detected by the photo diode with transimpedance amplifier that removes DC component and the received signal can be modelled in frequency domain after FFT as follows.

$$\tilde{\mathbf{y}} = \mathbf{F}_N \mathbf{H} \mathbf{F}_N^{-1} \tilde{\mathbf{d}} + \mathbf{F}_N \mathbf{n} \quad (11)$$

In the above,  $\mathbf{H} \in \mathbb{R}^{N \times N}$  denotes the channel matrix and  $\mathbf{n} \in \mathbb{R}^{N \times 1}$  represents Additive White Gaussian Noise (AWGN) vector with covariance  $\sigma_n^2 \mathbf{I}$ . Considering (10) in a convenient form by taking  $\tilde{\mathbf{H}} = \mathbf{F}_N \mathbf{H} \mathbf{F}_N^{-1}$  and  $\tilde{\mathbf{n}} = \mathbf{F}_N \mathbf{n}$  is given as,

$$\tilde{\mathbf{y}} = \tilde{\mathbf{H}} \tilde{\mathbf{d}} + \tilde{\mathbf{n}}. \quad (12)$$

Now the estimate of the data symbols  $\hat{\mathbf{d}}$  can be obtained by utilising Bayesian Gauss-Markov Theorem [15], and therefore, the Linear Minimum Mean Square Error (LMMSE) estimate is given by,

$$\hat{\mathbf{d}} = \mathbf{R}_{\tilde{\mathbf{d}}\tilde{\mathbf{d}}} \tilde{\mathbf{H}}^H (\tilde{\mathbf{H}} \mathbf{R}_{\tilde{\mathbf{d}}\tilde{\mathbf{d}}} \tilde{\mathbf{H}}^H + \mathbf{R}_{\tilde{\mathbf{n}}\tilde{\mathbf{n}}})^{-1} \tilde{\mathbf{y}}. \quad (13)$$

Here,  $\mathbf{R}_{\tilde{\mathbf{d}}\tilde{\mathbf{d}}} = \mathbb{E}[\tilde{\mathbf{d}}\tilde{\mathbf{d}}^H] = \sigma_q^2 \mathbf{Q}\mathbf{Q}^H$  and  $\mathbf{R}_{\tilde{\mathbf{n}}\tilde{\mathbf{n}}} = \mathbb{E}[\tilde{\mathbf{n}}\tilde{\mathbf{n}}^H] = N\sigma_n^2 \mathbf{I}$  specify corresponding covariance matrices for  $\tilde{\mathbf{d}}$  and  $\tilde{\mathbf{n}}$ . More precisely, (12) can be written as

$$\hat{\mathbf{d}} = \tilde{\mathbf{W}}\tilde{\mathbf{H}}^{-1}\tilde{\mathbf{y}}, \quad (14)$$

with a Wiener smoothing matrix given by

$$\tilde{\mathbf{W}} = \mathbf{Q}\mathbf{Q}^H \left( \mathbf{Q}\mathbf{Q}^H + \frac{N\sigma_n^2}{\sigma_q^2} (\tilde{\mathbf{H}}^H \tilde{\mathbf{H}})^{-1} \right)^{-1}. \quad (15)$$

Ultimately, the data symbols  $\hat{\mathbf{q}}$  are recovered by exerting  $\hat{\mathbf{q}} = \begin{bmatrix} \mathbf{I} & \mathbf{0} \end{bmatrix} \mathbf{P}^{-1} \hat{\mathbf{d}}$ . Accordingly, the overall process is summarised in the block diagram shown in Fig. 2, where the FFT is applied on the received signal followed by ZF equalisation and Wiener smoothing. Thereafter, the data is processed to recover original data symbols. Next, we present the simulation results for the Tx and Rx structures considered in this section.

### 2.3 Complexity Analysis

As per the algorithm, position matrix place data symbols  $\tilde{\mathbf{q}} \in \mathbb{C}^{N_m \times 1}$  on  $N_m$  sub-carriers from the available  $N$  sub-carriers. The proposed algorithm runs for the selection of optimal  $N_m$  sub-carriers from  $N$  sub-carriers. Hence, proposed algorithm has to run for  $\binom{N}{N_m}$  number of iterations for selecting optimal position matrix. For the given FFT size and constellation, the algorithm has to run only in the beginning of the communication. It is not required to run the algorithm every time for fixed system parameters. However, the algorithm has to re-run, only whenever a new communication with a different FFT size or a new PAM constellation, is established.

## 3. Simulation Results

The validity of the Ax-PAM based IM/DD systems is confirmed by performing elaborate simulations in MATLAB environment and compared with PAM-DMT and ACO-OFDM systems. Simulations for BER are carried under predominant AWGN environment in a VLC channel [12], [14]. For a fair BER comparison, equal data rates are contemplated for all the modulations under consideration. The proposed Ax-PAM is generated utilising a position matrix  $\mathbf{P}$  which is yielded by the Algorithm 1, that run only once in the beginning of the process for optimal case. However, to showcase the energy tuning, three different cases for  $\mathbf{T}$  are considered that yield different cost functions as per (10).

The process of energy tuning is illustrated in Fig. 4, where the time domain signals of Ax-PAM modulation are plotted in all different cases with different cost functions ( $C1 < C2 < C3$ ) obtained using (10). The difference among the time domain waveforms for cost function  $C1$  to  $C3$  can be observed in Fig. 4, where the peak values are reduced, while at the same time other sample values are increased. This means that the average energy of the signal is increased and at the same time the peak values are subsided which contribute to clipping power. This process of energy tuning effect the Peak to Average Power (PAPR) performance of the Ax-PAM system, which is compared with ACO-OFDM and PAM-DMT in Fig. 5(a). For PAPR comparison, the signals are lower clipped at zero and upper clipped at  $\infty$ . For Ax-PAM, a DC bias value of 7 dB is added before clipped at zero level to make it unipolar. The difference in performance can be observed for Ax-PAM system for different cases, which is due to increase in average energy of the signal and at the same time reduction in peak values. Further, a 2 dB gain in performance is also observed in  $C3$  case, compared to ACO-OFDM and PAM-DMT excluding the DC bias. For energy comparison 4-PAM is

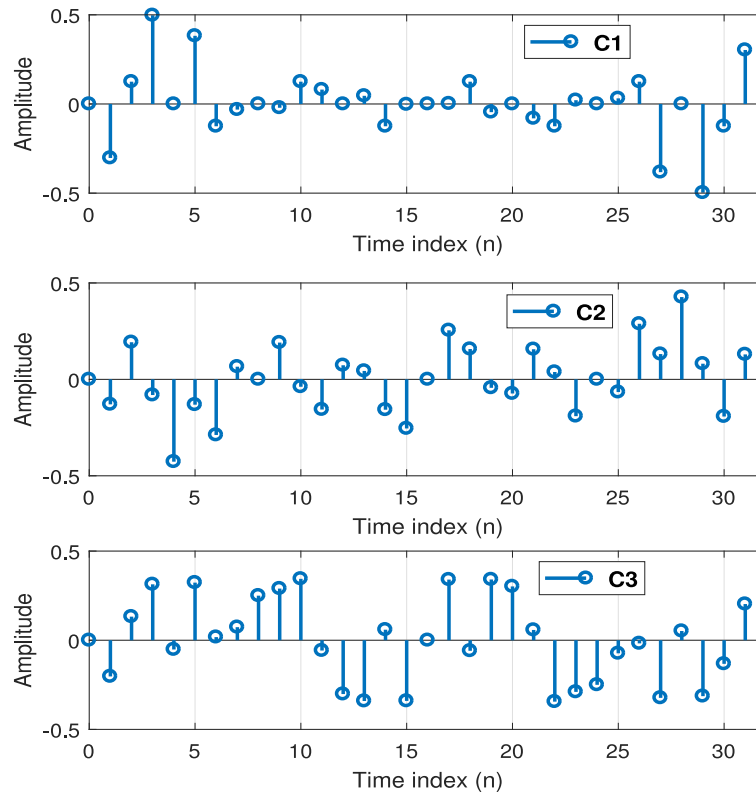


Fig. 4. Illustration of tunable energy in Ax-PAM time domain waveforms for different cost functions ( $C1 < C2 < C3$ ).

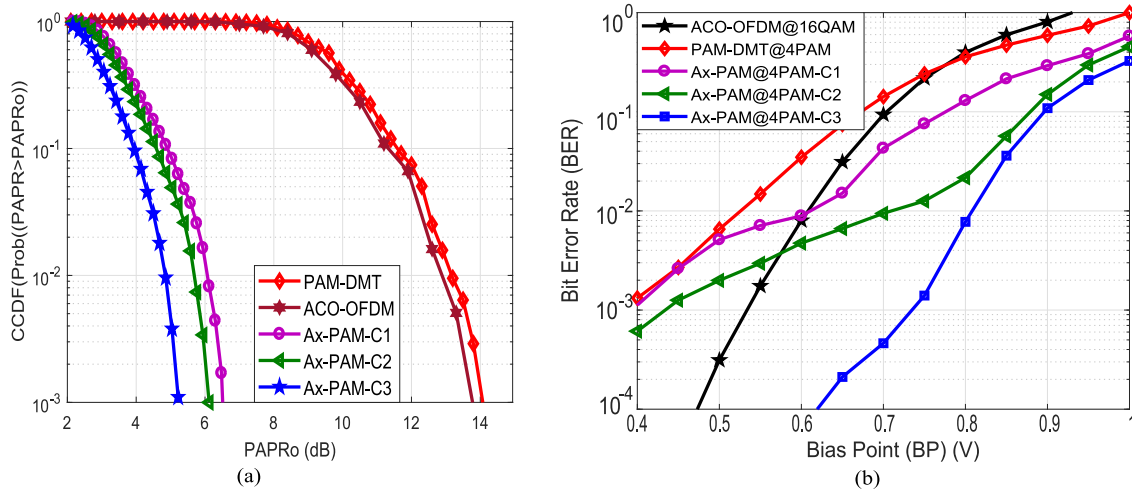


Fig. 5. (a) Comparison of PAPR performance of Ax-PAM at different cost functions with ACO-OFDM and PAM-DMT. (b) Comparison of achievable BER for ACO-OFDM, PAM-DMT and Ax-PAM at various Bias Points (BP) under clipping distortion.



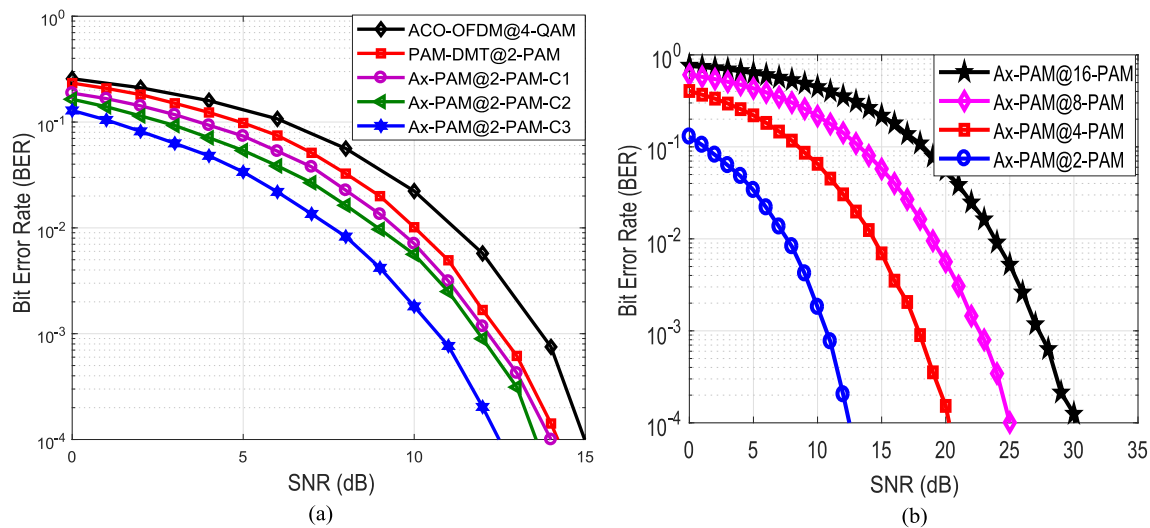


Fig. 6. (a) Comparison of BER for ACO-OFDM, PAM-DMT and Ax-PAM. (b) BER performance of Ax-PAM under C3 case for different order PAM constellations.

considered and the length ( $N_m$ ) of auxiliary and data symbols is considered as 16 which is valid for BER simulations also. An LED model with minimum turn on voltage of 0V and maximum allowable voltage 1V above which all values would be clipped is considered for all BER simulations. The effect of clipping distortion on the achievable BER performance at various Biasing Points (BP) is plotted in Fig. 5(b) for all the modulations with equal power. Since PAM-DMT and ACO-OFDM are contemplated, effect of upper clipping distortion has been examined. It is visualized that at a BP of 0.65 V, Ax-PAM with C3 has achieved a BER of  $2 \times 10^{-4}$  but ACO-OFDM attained  $3 \times 10^{-2}$  and PAM-DMT is limited to  $7 \times 10^{-2}$  only due to more clipping. It can be seen from the Fig. 5(b) that, for the cost function C3 case, Ax-PAM achieves less BER than other two cost function cases due to the reduction in the peak values, which in turn reduce the clipping power.

The simulated BER for Ax-PAM is depicted in Fig. 6(a) along with PAM-DMT and ACO-OFDM. A bias value of 0.4V is used for Ax-PAM and 0.1V is utilized for ACO-OFDM and PAM-DMT as they are inherently unipolar. This is to balance the optical power constraints as in [16]. The comparison illustrates that an error of  $2 \times 10^{-4}$  is attained at Signal to Noise ratio (SNR) of 12 dB for Ax-PAM with C3, which is less by 2 dB and 3 dB with respect to PAM-DMT and ACO-OFDM respectively. This is due to the improvement in the PAPR performance that comes with energy tuning. The BER performance of Ax-PAM system for other cost functions is also depicted in the Fig. 6(a).

Fig. 6(b) depicts the comparison between BER performance of the proposed Ax-PAM for different orders of M-PAM constellations. It can be viewed that to get an error of  $2 \times 10^{-4}$ , a SNR of 12 dB, 19 dB, 24 dB, and 29 dB are taken by 2, 4, 8, and 16-PAM constellations respectively. This is due to the decrease in euclidean distance between symbols with increase in modulation order of constellation. Next, we present the experimental results for the proposed scheme.

#### 4. Experimental Results

Recently, the validation of proposed theory or algorithms through experiments has gained popularity due to accessibility with USRP hardware devices. In this section, we first describe the VLC test bed designed with USRPs, which is used for the implementation of proposed modulation. After that, the experimental results under various conditions are presented with detailed explanation. The processing steps incurred in the implementation are illustrated in the block diagram shown in Fig. 7, in which the test bed is also displayed in the inset.

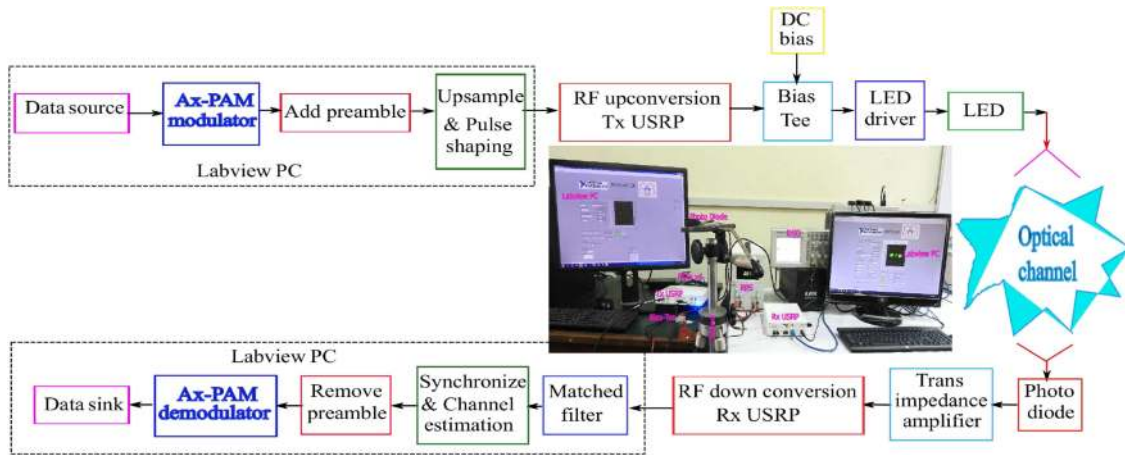


Fig. 7. Block diagram illustration of experimental procedure used for Ax-PAM implementation (Inset shows VLC testbed used in the implementation).

TABLE 1  
Experimental Set-Up Parameters

Name of the parameter	Value	Name of the parameter	Value
Modulation order (M)	4	Samples in One Frame	25,904
Number of sub carriers (M)	32	USRP IQ sampling rate	8M
Number of data Ax-PAM symbols	400	PD-Thorlabs-PDA8A	(DC-50MHz), 0.56A/W @ 820 nm
Preamble length	128	LED	16 W
Zeropad length on each side of frame	8	Link distance (cm)	0.5m to 1.5m
Pulse shaping (RRC) length	8	Average electrical transmitted power (mW)	4mW
Roll off factor- $\alpha$	0.2	USRP with LFTx and LFRx daughter boards	Ettus X300, N210
Oversampling factor (L)	2	Bias Tee	ZFBT-6GW-FT+

The base band processing of the proposed modulated signal is done in the Lab-view software, where the oversampled Ax-PAM modulated signal is pulse shaped by using Nyquist Root Raised Cosine (RRC) pulse after preamble addition. The pulse shaped signal from Lab-view PC is given to transmitter USRP X300 as per In-phase (I)/Quadrature-phase(Q) sampling rate, which is processed by Digital to Analog (DAC) converter that is implemented on the FPGA present in USRP mother board. Thereafter, the transmitted data packet is carried on a high frequency RF carrier signal to which a DC bias is added by Bias Tee to make it unipolar. The transmitted packet duration is determined by dividing data frame size after pulse shaping with transmit IQ sample rate. The unipolar RF signal from Bias Tee is then modulate the LED intensity, which is perceived by Photo Diode (PD), that send the signal to receiver USRP N210 in electrical form. The receiver USRP perform counter steps to transmitter USRP and transfer the signal to PC for receiver base band processing steps as shown in Fig. 7. Here it should be noted that the capture time of the receiver USRP must be greater than the transmitted packet duration which ensures sufficient number of samples are attained at the detector.

The experimental set-up parameters used in the proposed implementation are tabulated in Table 1. In this case, the number of Ax-PAM symbols generated in each frame are kept at 400 each with 32 data subcarriers. A known preamble of length 128 is added for each frame along with

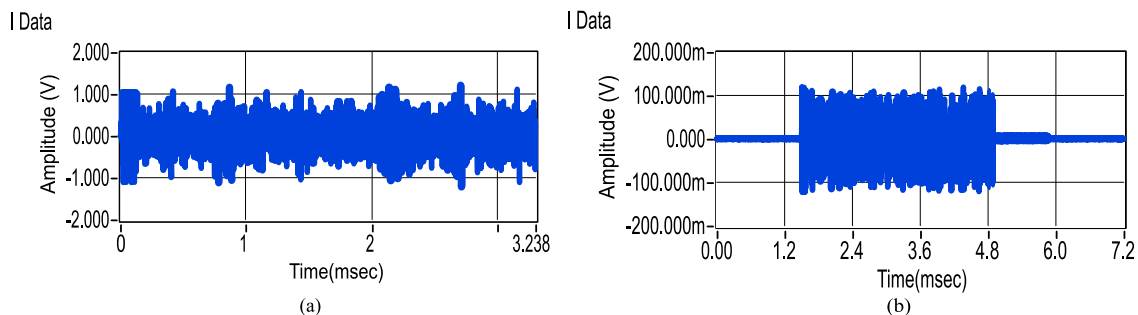


Fig. 8. A plot of time domain signals. (a) Transmitted data packet. (b) Received data packet.

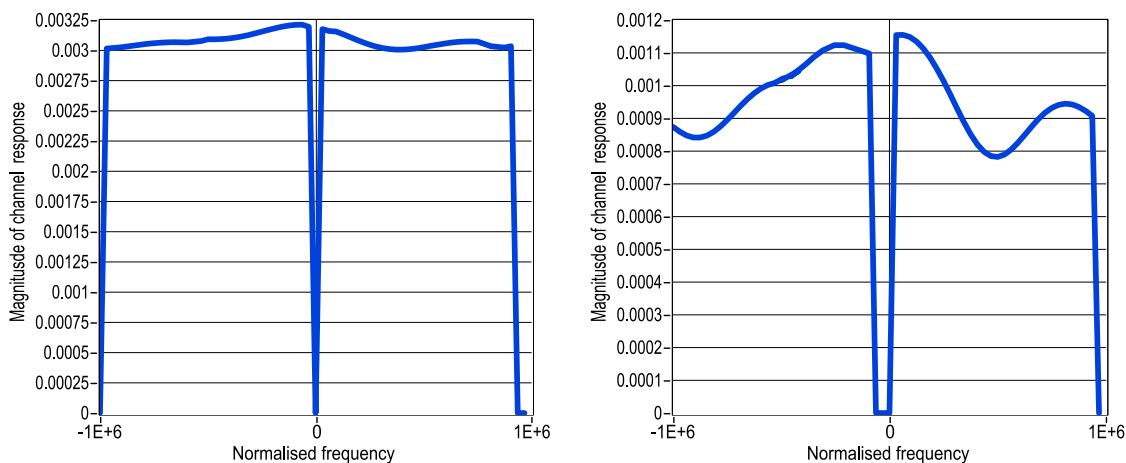


Fig. 9. Measured channel frequency response at different distances between LEDs and PD: (a)  $d = 0.5$  m and (b)  $d = 1.5$  m.

zero padding for synchronisation and channel estimation. The frame is oversampled by a factor equal to 2 and passed through RRC pulse shaping filter of length 8. This constitutes a frame of size 25,904. The resultant signal is given to transmitter USRP with a IQ sampling rate of 8M samples per second. The ratio of frame size to the IQ sample rate determines the transmitted packet duration as 3.238 ms. The transmitted data packet is shown in Fig. 8(a). This data packet is transmitted through RF carrier generated by USRP which modulates the LED intensity. Based on the variations in the light intensity level, PD produces electrical signal that is processed to undergo down conversion and Analog to Digital Conversion (ADC) steps by the receiver USRP. Thereafter, the data packet is transferred to Lab-view PC which is depicted in Fig. 8(b). It can be noticed that when compared with transmitted data packet, there is a delay of 1.6 ms in received time and 10 dB degradation in amplitude in the received data packet. These are due to the characteristics of channel attenuation and propagation delay. To manifest the VLC channel characteristics, the channel frequency responses are measured at different distances  $d = 0.5$  m and  $d = 1.5$  m between transmit LED and receive PD and illustrated in Fig. 9(a) and (b), respectively. Since the channel is measured in real time scenario, the channel response tends to diffuse due to the presence of both LoS and Non LoS (NLoS) components, where the ideal response would be perfectly flat. This diffusion due to LoS and NLoS components increases with the separation distance between LED transmitter and photo diode receiver. It is seen that at a smaller distance, the channel frequency response is almost flat and resembles ideal frequency response. On the other hand as distance increases, the channel response tends to diffuse which is due to the more reflective components that come into the PD. In addition to the above, the transmitted signal constellation for 4-PAM is shown in Fig. 10, which

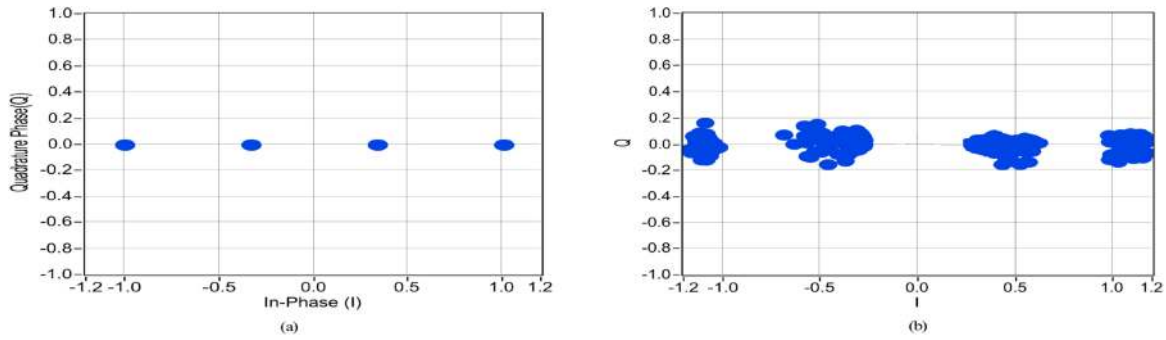


Fig. 10. Figure shows (a) transmitted and (b) received constellation for 4-PAM at 20 dB SNR with  $d = 1.5$  m.

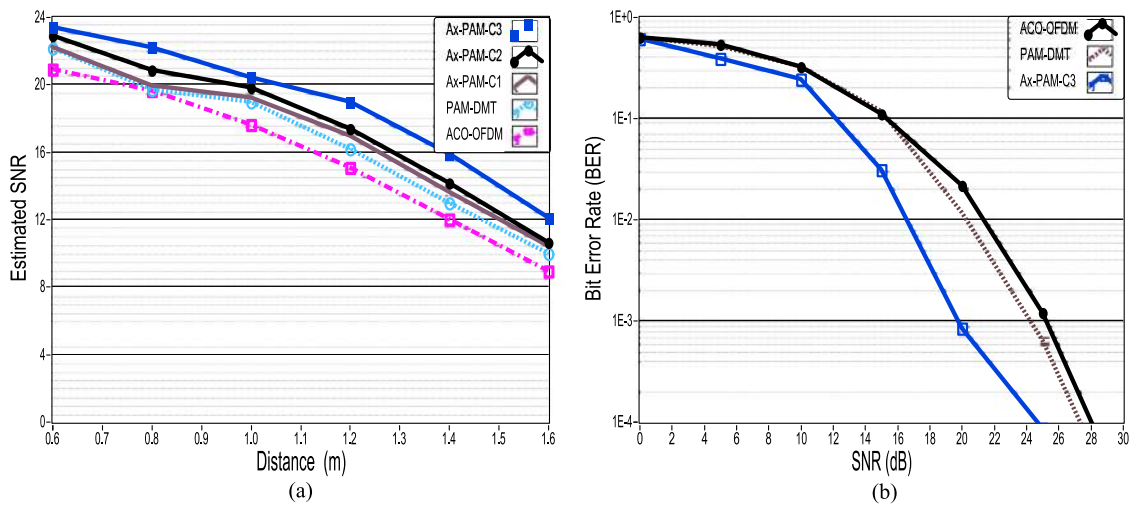


Fig. 11. Performance comparison of (a) estimated SNR at receiver with respect to distance and (b) achieved BER with respect to SNR (dB) between Ax-PAM and PAM-DMT.

will be transmitted in the form of a packet by using transmit USRP. Now coming back to receiver, the received data packet undergo different processing steps like matched filtering, synchronisation and channel estimation as shown in receiver part of Fig. 7. Finally, the received constellation for the demodulated symbols at 20 dB SNR with  $d = 1.5$  m is plotted in Fig. 10(b). As a performance metric for measuring the distortion in the received constellation, Error Vector Magnitude (EVM) is calculated similar to the approach in [17]. EVM over a Ax-PAM symbol is calculated by Root Mean Square (RMS) value of the magnitudes obtained by subtracting received constellations from the corresponding ideal constellation. For the considered 4-PAM over a burst of 50 Ax-PAM symbols, a low value of nearly 11% EVM and a higher value of around 23% EVM is observed.

In addition to the above, estimated SNR computed at the receiver is a vital parameter to comment on detection accuracy for any waveform transmitted in real channel conditions. The estimated SNR is calculated by mean square error obtained in the computation of channel estimation. Fig. 11(a) depicts the variation of estimated SNR comparison at the receiver with respect to distance ( $d$ ) between LED and PD for the proposed scheme for different cost functions ( $C1 < C2 < C3$ ) with traditional DMT schemes. It is observed that the proposed waveform outperforms traditional PAM-DMT and ACO-OFDM as the link distance ( $d$ ) increases. This is due to the improvement in PAPR performance that minimize clipping noise power as reported from Fig. 5. Furthermore, the achieved BER at different SNR values for the proposed scheme (with cost function C3) is also

compared with PAM-DMT and ACO-OFDM in Fig. 11(b). This shows that the proposed scheme surpasses traditional schemes and also shows a close match to simulation result. It is seen that the improvement in BER performance for Ax-PAM is due to good estimated SNR values. In the comparison, for equal spectral efficiency corresponding to 4-PAM in PAM-DMT and proposed scheme, 16-QAM is considered for ACO-OFDM.

## 5. Conclusion

The upcoming VLC systems need to cope up with power requirements and clipping distortion. To render these services, a novel waveform named Ax-PAM that relies on tunable energy auxiliary symbols, instead of hermitian symmetry to produce real signal is introduced and implemented using VLC test bed designed using USRPs. Along with 2 dB gain in BER performance with respect to PAM-DMT and ACO-OFDM, the proposed waveform has shown good performance even under clipping distortion in simulations. The simulated BER result is validated through experiment in real channel conditions and further shown that proposed waveform outperforms PAM-DMT and ACO-OFDM in terms of estimated SNR at the receiver.

## Acknowledgment

The authors would like to thank National Instruments (NI) for providing additional support.

---

## References

- [1] T. Zhang, Y. Zou, J. Sun, and S. Qiao, "Design of PAM-DMT-based hybrid optical OFDM for visible light communications," *IEEE Wireless Commun. Lett.*, vol. 8, no. 1, pp. 265–268, Feb. 2018.
- [2] S. Vappangi and V. M. Vakamulla, "Synchronization in visible light communication for smart cities," *IEEE Sensors J.*, vol. 18, no. 5, pp. 1877–1886, Mar. 2018.
- [3] K. Mallick, R. Mukherjee, B. Das, G. C. Mandal, and A. S. Patra, "Bidirectional hybrid OFDM based wireless-over-fiber transport system using reflective semiconductor amplifier and polarization multiplexing technique," *AEU-Int. J. Electron. Commun.*, vol. 96, pp. 260–266, 2018.
- [4] K. Mallick, P. Mandal, G. C. Mandal, R. Mukherjee, B. Das, and A. S. Patra, "Hybrid mmw-over fiber/OFDM-FSO transmission system based on doublet lens scheme and polmux technique," *Opt. Fiber Technol.*, vol. 52, 2019, Art. no. 101942.
- [5] M. Huemer, C. Hofbauer, and J. B. Huber, "The potential of unique words in OFDM," in *Proc. 15th Int. OFDM-Workshop*, 2010, pp. 140–144.
- [6] A. Onic and M. Huemer, "Direct versus two-step approach for unique word generation in UW-OFDM," in *Proc. 15th Int. OFDM-Workshop*, 2010, pp. 145–149.
- [7] S. A. Cheema, M. Wolf, M. Huemer, and M. Haardt, "Unique word DMT schemes using real-valued constellations for IM/DD optical systems," *IEEE Photon. Technol. Lett.*, vol. 30, no. 10, pp. 935–938, May 2018.
- [8] S. A. Cheema, E. R. Balda, M. Wolf, and M. Haardt, "Unique word DMT schemes for optical systems with intensity modulation and direct detection," *J. Lightw. Technol.*, vol. 35, no. 18, pp. 3862–3869, Sep. 2017.
- [9] S. P. Valluri and V. V. Mani, "Investigation of blind CFO estimation for GFDM system using universal software radio peripheral: theory, simulations and experiments," *IET Commun.*, vol. 13, no. 13, pp. 1936–1944, Aug. 2019.
- [10] S. Valluri and V. Mani, "Joint channel mitigation and side information estimation for GFDM systems in indoor environments," *AEU—Int. J. Electron. Commun.*, vol. 95, pp. 146–154, 2018.
- [11] S. P. valluri and V. V. Mani, "Demonstration of effect of oversampling on jitter removal for Multitaper GFDM system using SDR," in *Proc. Int. Conf. Adv. Technol. Commun.*, Oct. 2018, pp. 168–173.
- [12] V. Kishore and V. Mani, "A DC biased optical generalised frequency division multiplexing for IM/DD systems," *Phys. Commun.*, vol. 33, pp. 115–122, 2019.
- [13] D. D. B. F. a. Dr. Zbigniew Michalewicz, *How to Solve It: Modern Heuristics*, 2nd ed. Berlin, Germany: Springer, 2004.
- [14] S. R. Z. Ghassemlooy, W. Popoola, *Optical Wireless Communications: System and Channel Modelling With MATLAB*, 1st ed. Boca Raton, FL, USA: CRC Press, 2012.
- [15] S. M. Kay, *Fundamentals of Statistical Signal Processing, Volume I: Estimation Theory*. Englewood Cliffs, NJ, USA: Prentice-Hall, 1993.
- [16] S. Dimitrov, S. Sinanovic, and H. Haas, "Clipping noise in OFDM-based optical wireless communication systems," *IEEE Trans. Commun.*, vol. 60, no. 4, pp. 1072–1081, Apr. 2012.
- [17] G. C. Mandal, R. Mukherjee, B. Das, and A. S. Patra, "A full-duplex WDM hybrid fiber-wired/fiber-wireless/fiber-VLC/fiber-IVLC transmission system based on a self-injection locked quantum dash laser and a rsoa," *Opt. Commun.*, vol. 427, pp. 202–208, 2018.